

*Full Length Research Paper*

# Fuzzy B-spline algorithm for 3-D lineament reconstruction

**Maged Marghany**

Institute of Geospatial Science and Technology (INSTEG), Universiti Teknologi Malaysia 81310 UTM, Skudai, Johore Bahru, Malaysia. E-mail: [maged@utm.my](mailto:maged@utm.my), [magedupm@hotmail.com](mailto:magedupm@hotmail.com).

Accepted 21 March, 2012

**Lineaments are vital geological features that play the role of a key indicator for ground water and petroleum searching. At present, there is no study that has utilised remote sensing satellite data to reconstruct three dimensional (3-D) lineament visualization in the United Arab Emirates (UAE). This work aimed at reconstructing a (3-D) lineament visualization from multispectral remote sensing such as LANDSAT TM. In doing so, the fuzzy B-spline algorithm was used to reconstruct 3-D from two dimensional (2-D) LANDSAT TM 7 satellite data. Prior to the fuzzy B-spline algorithm, image enhancement contrast, stretching and linear enhancements were applied to acquire an excellent visualization. In addition, automatic detection algorithm of Canny was performed to extract linear features in multispectral remote sensing data, that is, lineaments, fractures. Uncertainty digital elevation model (DEM) was performed by using fuzzy B-spline algorithm to map spatial lineament variation in 3-D. Further, a fuzzy B-spline algorithm was used to reconstruct 3-D visualization of lineament with standard error of mean of 0.12 and bias of 0.23. In conclusion, fuzzy B-spline provides excellent promising for 3-D geological features reconstruction from two dimensional (2-D) remote sensing satellite data.**

**Key words:** Lineament, 3D visualizations, DEM, multispectral remotely sensed data, LANDSAT TM.

## INTRODUCTION

Approximately 90% of the United Arab Emirate (UAE) is experiencing scarcity of underground water. Highly complex topography features exist in eastern side of UAE which contains huge numbers of Lineaments and fractures. Discontinuities of groundwater flow, rainfall recharge and salinity intrusions recurred due to lineaments and fractures. Furthermore, lineaments play an important role in structural controls of groundwater vertical and lateral flow along fault and bedding plans. In this region, lineaments are located in the mountainous eastern part of UAE. They consist of fault zones, fractures that affect ground waters recharges, especially in the area adjacent to the Oman Mountain (Semere and Ghebreab, 2006).

Conventional techniques of lineament extraction and mapping are conducted manually. The manual techniques are challenging task that are time consuming and require many labours. Because of the Earth's complex topography, visual interpretation is an imperfect approach for lineament extraction from aerial photography and

remote sensing data especially with macroscale focus (Mallast et al., 2011). Thus, researchers and scientists have developed semi automated and automated algorithms to acquire precisely lineament features detection and mapping from remotely sensed data. Mallast et al. (2011) also stated that semi-automatic and automatic algorithms are involved in morphological filter and either in linear or non-linear algorithm. Other algorithms are included edge tracing and linking methods and knowledge based systems (Mallast et al., 2011).

In referring to Katsuaki et al. (1995), Moore et al. (1998) and Walsh and Clark (2000), the lineament information extractions in satellite images can be divided broadly into three categories: (i) Lineament enhancement and lineament extraction for characterization of geologic structure; (ii) the image classification to perform geologic mapping or to locate spectrally anomalous zones attributable to mineralization (Mostafa and Quay, 1995; Szen and Toprak, 1998; Islam et al., 2011a, b, c) and (iii) the superposition of satellite images and multiple data such

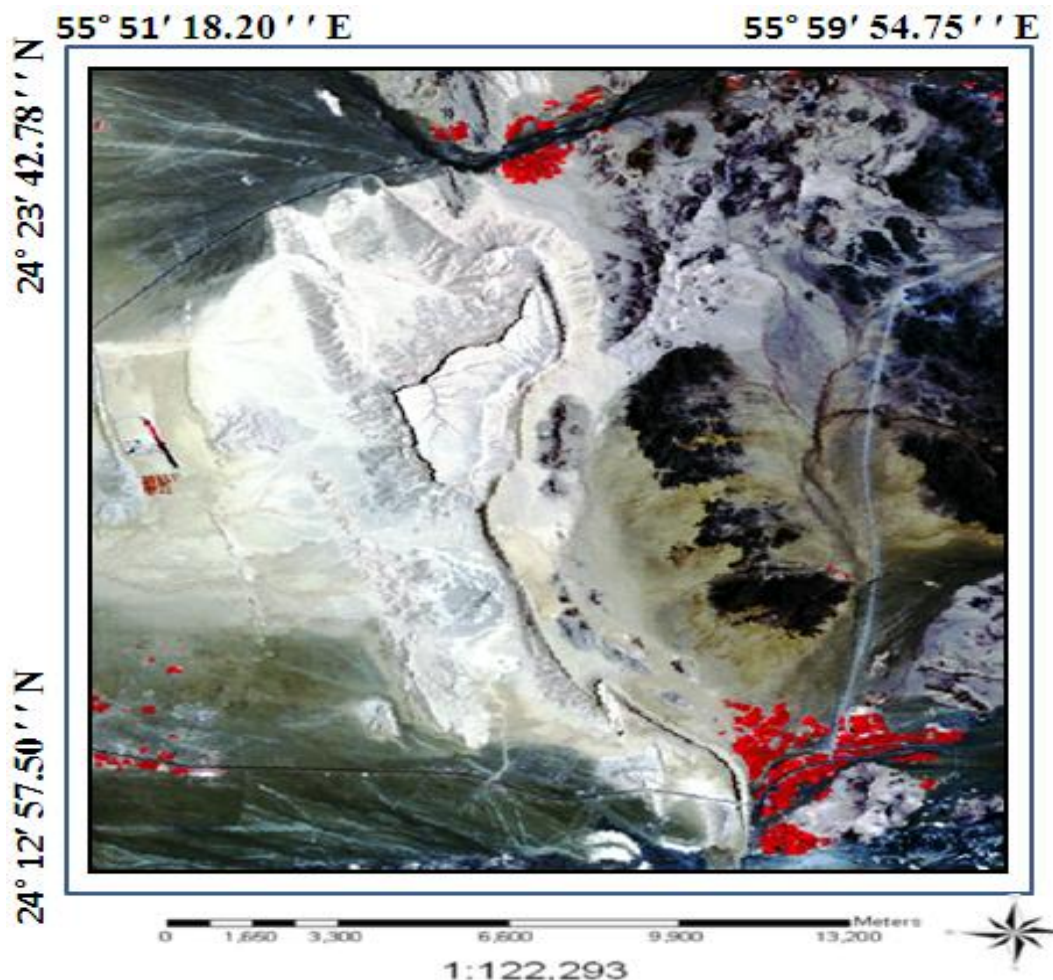


Figure 1. Location of Study area.

as geological, geochemical, and geophysical data in a geographical information system (Novak and Soulakellis, 2000; Semere and Ghebreab, 2006; Islam et al., 2012a, b, c; Munir et al., 2012). Furthermore, remote sensing data assimilation in real time could be a bulk tool for geological feature extraction, mapping and structural reconstruction (Islam et al., 2012d, e, f; Jameel et al., 2012a, b, c). Thus, several investigations are currently underway on the assimilation of both passive and active remotely sensed data into automatic detection of significant geological feature (for example, lineament). Edge automatic detection algorithms such as the Laplacian, Sobel and Canny are the major geomatica tool for lineament investigation in remotely sensed data. In this study, there is integration of different automatic detection algorithms to develop a new approach for lineament detection and mapping. This work hypothesized that lineament features can be reconstructed in three dimensional (3-D) visualization. In this regard, the Canny algorithm can be used as semi-automatic tool to discriminate between lineament and surrounding geological

features in optical remotely sensed satellite data. In addition, uncertainty of DEM model can be overcome by using the fuzzy B-spline algorithm to map spatial lineament variation in 3-D visualization. The main objective of this study is to visualize lineament spatial variation in 3-D using fuzzy B-spline algorithm with comparison with 2-D lineament mapping using Canny algorithm.

## METHODOLOGY

### Study area

The study area is located in Sharjah Emirates about 70 Km from Sharjah city. It is considered as an alluvium plain in the central area of UAE and it covers an area of 1800 Km<sup>2</sup> (60 km x 30 km) within boundaries of latitudes 24° 12'N to 24° 23'N and longitudes 55° 51'E to 55° 59' E (Figure 1). The northern part of UAE is formed of the Oman mountains and the marginal hills extends from the base of the mountains and (alluvium plain) to the south western sand dunes (Figures 2 and 3) such features can be seen clearly in Wadi Bani Awf, Western Hajar (Figure 2). The land's geomorphology



**Figure 2.** Geologic fault feature along Oman mountain.



**Figure 3.** Dune forms on Oman mountain base.

consists of its structural, fluvial and Aeolian forms (sand dunes). In line with Marghany et al. (2009), structural form is broad of the Oman mountains and JabalFayah (Figure 3) which are folded structure due collision of oceanic crust and Arabian plate (continental plate). Furthermore, the mountain is raised higher than 400 m above sea level and exhibit parallel ridges and high-tilted beds. Many valleys are cut down the mountains, forming narrow clefts and there are also intermittent basins caused by differential erosion. In addition, the valley bases are formed small caves. Stream channels have been diverted to the southwest and they deposited silt in the tongue-shaped which lies between the dunes. Further, Aeolian forms are extended westwards from the Bahada plain, where liner dunes run towards the southwest direction in parallel branching pattern (Figure 3) with relative heights of 50 meters. Nevertheless, the heights are decreased towards the southeast due to a decrease in sand supply and erosion caused by water occasionally flowing from the Oman mountains (Marghany and Mazlan, 2010).

### Data sets

This study uses two sort of data. First, is the satellite data which comprise LANDSAT Enhanced Thematic Mapper (ETM) image with pixel resolution of 30 m which was acquired at 14:07 on 18 December 2004 (Figure 2). It covers area of 24° 23' N, 55° 52' E to 24° 17' N and 55° 59' E (Figure 2). Landsat sensors have a moderate spatial-resolution. It is in a polar, sun-synchronous orbit, meaning it scans across the entire earth's surface. With an altitude of 705 kilometres +/- 5 kilometres, it takes 232 orbits, or 16 days, to do so. The main features of LANDSAT-7 includes:

1. A panchromatic band with 15 m (49 ft) spatial resolution (band 8)
2. Visible (reflected light) bands in the spectrum of blue, green, red, near-infrared (NIR), and mid-infrared (MIR) with 30 m (98 ft) spatial resolution (bands 1 to 5, 7)
3. A thermal infrared channel with 60 m spatial resolution (band 6)
4. Full aperture, 5% absolute radiometric calibration (Robinson et al., 2007)

Second, is the ancillary data which contain digital topographic, geological maps, well logs and finally ground water data. Furthermore, ancillary data such as topography map of scale 1: 122,293 was used to generate DEM of selected area. Bands 1, 2, 3, 5 and 7 are selected to achieve the objective of this study. According to Marghany et al. (2009), these bands can provide accurate geological information. Finally, the DEM was acquired from SRTM data.

### Lineament extraction procedures

This involved three image processing procedures: (i) image enhancement, (ii) semi-automatic lineament feature detections using Canny algorithm; and (iii) DEM reconstruction using SRTM data and fuzzy B-spline algorithm.

### Histogram equalization

Following Marghany et al. (2009), histogram equalization is applied to LANDSAT TM image to obtain high quality image visualization. An image histogram is an analytic tool used to measure the amplitude distribution of pixels within an image. For example, a histogram can be used to provide a count of the number of pixels at amplitude 0, the number at amplitude 1 and so on. By analyzing the distribution of pixel amplitudes, you can gain some information about the visual appearance of an image. A high-contrast image contains a wide distribution of pixel counts covering the entire amplitude range. A low contrast image has most of the pixel amplitudes congregated in a relatively narrow range (Süzen and Toprak, 1998; Gonzalez and Woods, 1992).

### Canny algorithm

According to Canny (1986), the Canny edge detector uses a filter based on the first derivative of a Gaussian, because it is susceptible to noise observed on the unprocessed image data, so to begin with, the raw image is convolved with a Gaussian filter. The result is a slightly blurred version of the original which is not affected by a single noisy pixel to any significant degree. According to Deriche (1987), the edge detection operator (for example, Roberts, Prewitt, Sobel) returns a value for the first derivative in the horizontal direction ( $G_y$ ) and the vertical direction ( $G_x$ ). From this the edge gradient and direction ( $\Theta$ ) can be determined:

$$|G| = \sqrt{G_x^2 + G_y^2} \quad (1)$$

In fact, Equation 1 is used to estimate the gradient magnitude (edge strength) at each point which can be found on the edge strength by taking the gradient of the image. Typically, an approximate magnitude is computed using:

$$|G| = |G_x| + |G_y| \tag{2}$$

Equation 2 is quickly computed and thus results to:

$$\theta = \arctan \left( \frac{G_y}{G_x} \right) \tag{3}$$

The direction of the edge  $\theta$  is computed using the gradient in the  $G_x$  and  $G_y$  directions. However, an error will be generated when sum  $X$  is equal to zero. So in the code, there has to be a restriction set whenever this takes place. Whenever the gradient ( $G$ ) in the  $x$  direction is equal to zero, the edge direction has to be equal to 90 degrees or 0 degrees, depending on what the value of the gradient in the  $y$ -direction is equal to. If  $G_y$  has a value of zero, the edge direction will be equal to 0 degrees. Otherwise, the edge direction will be equal to 90 degrees (Deriche, 1987).

According to Gonzalez and Woods (1992), three criteria are used to improve edge detection. The first and most obvious is low error rate. It is important that edges occurring in images should not be missed and that there be NO responses to non-edges. The second criterion is that the edge points be well localized. In other words, the distance between the edge pixels as found by the detector and the actual edge is to be at a minimum. A third criterion is to have only one response to a single edge, this was implemented because the first 2 were not substantial enough to completely eliminate the possibility of multiple responses to an edge (Canny, 1986).

**The fuzzy B-splines algorithm**

The fuzzy B-splines (FBS) are introduced allowing fuzzy numbers instead of intervals in the definition of the B-splines. Typically, in computer graphics, two objective quality definitions for fuzzy B-splines are used: triangle-based criteria and edge-based criteria (Marghany et al., 2009). A fuzzy number is defined using interval analysis. There are two basic notions that was combine together: confidence interval and presumption level. A confidence interval is a real values interval which provides the sharpest enclosing range for current gradient values.

An assumption  $\mu$  -level is an estimated truth value in the  $[0, 1]$  interval seen on our knowledge level of the topography elevation gradients (Anile, 1997). The 0 value corresponds to minimum knowledge of topography elevation gradients and 1 to the maximum topography elevation gradients. A fuzzy number is then prearranged in the confidence interval set, each one related to an assumption level  $\mu \in [0, 1]$ . Moreover, the following must hold for each pair of confidence intervals which define a number:  $\mu > \mu' \Rightarrow d > d'$ .

Based on the spatial variation of the topography elevation gradients, the fuzzy B-spline algorithm is used to compute the function  $f$  (Marghany et al., 2010). Follow Marghany et al. (2010),  $d(i,j)$  is the topography elevation value at location  $i,j$  in the region  $D$  where  $i$  is the horizontal and  $j$  is the vertical coordinates of a grid of  $m$  times  $n$  rectangular cells. Let  $N$  be the set of eight neighbouring cells. The input variables of the fuzzy are the amplitude differences of water depth  $d$  defined by (Anile et al., 1997):

$$\Delta d_N = d_i - d_0, N = 1, \dots, 4 \tag{4}$$

Following Rövid et al. (2004), Equation 4 represent topography elevation in 2-D, in order to reconstruct fuzzy values of topography elevation in 3-D, then fuzzy number of digital elevation in  $z$  coordinate is estimated by the following equation proposed by Russo (1998) and Marghany et al. (2010),

$$d_z = \Delta \mu \text{MAX} \{ m_{LA} |d_{i-1,j} - d_{i,j}|, m_{LA} |d_{i,j-1} - d_{i,j}| \} \tag{5}$$

where  $d_z$  fuzzy set of digital elevation values in  $z$  coordinate which is a function of  $i$  and  $j$  coordinates, that is,  $d_z = F(d_i, d_j)$ .

Fuzzy number  $F_O$  for DEM in  $i,j$  and  $z$  coordinates, then can be given by

$$F_O = \{ \min(d_{z_0}, \dots, d_{z_\Omega}), \max(d_{z_0}, \dots, d_{z_\Omega}) \} \tag{6}$$

where  $\Omega = 1, 2, 3, 4,$

The fuzzy number of DEM  $F_O$  then is defined by B-spline in order to reconstruct 3-D of digital elevation. In doing so, B-spline functions including the knot positions and the fuzzy set of control points were constructed. The requirements for B-spline surface are set of control points, set of weights and three sets of knot vectors which are parameterized in the  $p$  and  $q$  directions.

Following Marghany et al. (2009b; 2010), a fuzzy number is defined, whose range is given by the minimum and maximum values of digital elevation along each kernel window size. Furthermore, the identification of a fuzzy number is acquired to summarize the estimated digital elevation data in a cell and it is characterized by a suitable membership function. The choice of the most appropriate membership is based on triangular numbers which are identified by minimum, maximum and mean values of digital elevation estimated. Furthermore, the membership support is the range of digital elevation data in the cell and whose vertex is the median value of digital elevation data (Anile et al., 1997).

**RESULTS AND DISCUSSION**

Figure 4 shows the output result mapping of lineaments using composite of bands 3, 4, 5 and 7 in LANDSAT TM satellite data. The appearance of lineaments in LANDSAT TM satellite image are clearly distinguished. In addition, the area adjacent to the mountainous area from Manamh (northward) and Flili village (southward) has high density of lineaments due to the westward compressive force between the oceanic crust and Arabian plate, such as, fractures and faults and drainage pattern that runs in the buried fault plains (filled weathered materials coming from Oman mountains) (Figure 4). The lineaments are associated with fractures and faults which are located in northern part of Figure 4.

In fact, Canny algorithm was first used to smooth the image to eliminate noise. It then finds the image gradient to highlight regions with high spatial derivatives. The algorithm tracks along these regions and suppresses any pixel that is not at the maximum (non-maximum suppression). The gradient array was further reduced by

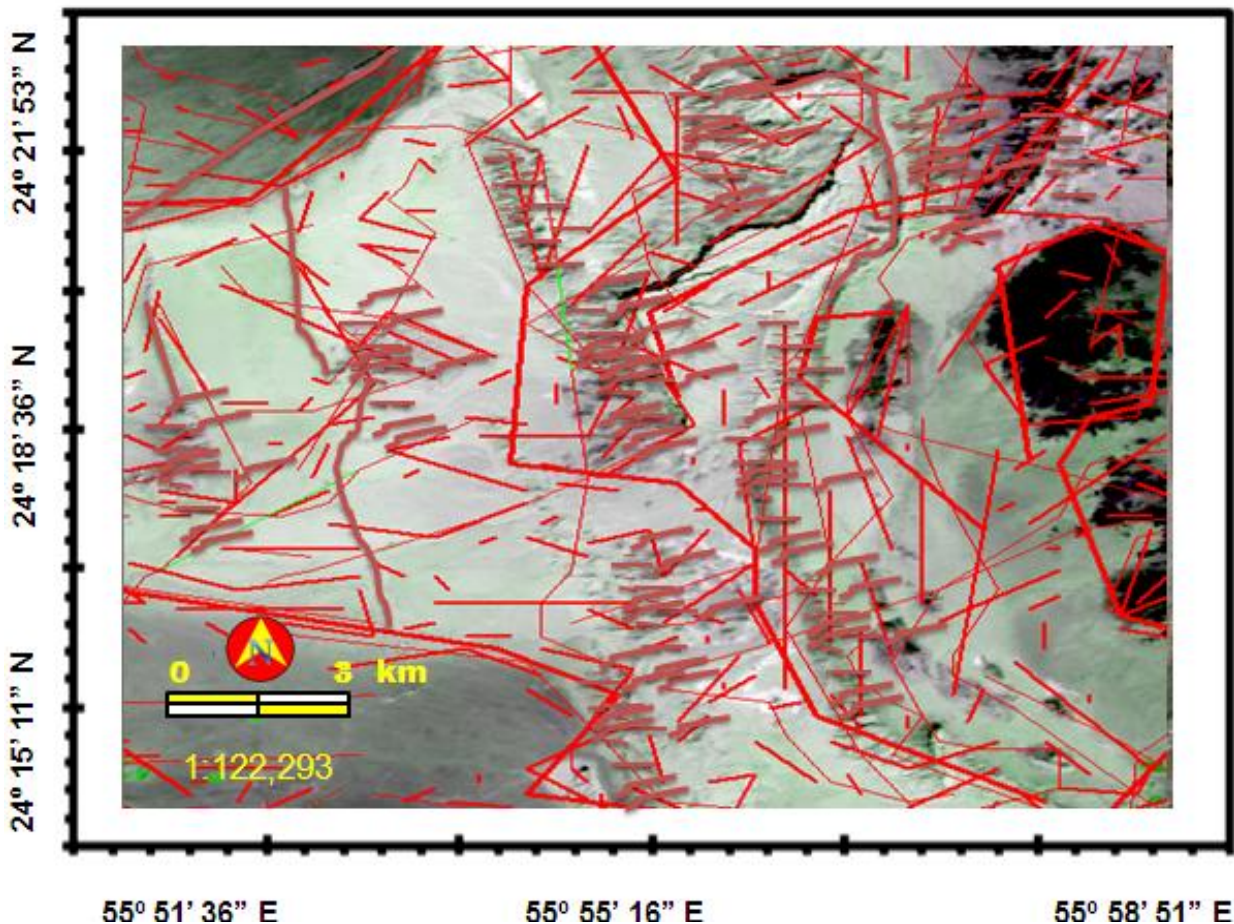


Figure 4. Lineament mapping using Canny algorithm.

hysteresis. The hysteresis is used to track along the remaining pixels that have not been suppressed (Deriche, 1987). Hysteresis uses two thresholds and if the magnitude is below the first threshold, it is set to zero (made a non-edge).

According to Marghany et al. (2009), LANDSAT TM data can be used to map geological features such as lineaments and faults. This could contribute to the fact that the composite of bands 3, 4, 5 and 7 in LANDSAT TM satellite data are appropriate for mapping of geologic structures (Katsuaki et al, 1995; Novak and Soulakellis, 2000; Marghany et al., 2009). Consequently, the ground resolution cell size of LANDSAT TM data is about 30 m. This confirms the study of Robinson et al. (2007).

Figure 5 shows the digital elevation model derived from SRTM data that covers an area of approximately 11 km<sup>2</sup>. Clearly, DEM varies between 319 and 929 m and maximum elevation value of 929 m was found in the northeast direction of UAE. Therefore, SRTM ensures the production of DEM with a root mean square error of 16 m (Nikolakopoulos et al., 2006). In addition, Oman mountain has the highest DEM value of 929 m which is shown to be parallel with the coastal zone of Arabian Gulf. The

DEM is dominated by spatial variation of the topography features, such as, ridges, sand dunes and steep slopes. As the steep slopes are clearly seen within DEM of 400 m (Figure 5). According to Zaineldeen (2011), the rocks are well bedded massive limestones with some replacement chert band sand nodules. The limestone has been locally dolomitized.

According to Robinson et al. (2007), TM bands 7 (2.08 to 2.35  $\mu$ m), 4 (0.76 to 0.90  $\mu$ m) and 2 (0.50 to 0.60  $\mu$ m) are appropriate for geological features detection because they have low-correlation and produce high-contrast. In this regard, band 2 was useful for rock discrimination, band 4 for land/water contrasts and band 7 for discrimination of mineral and rock types. Furthermore, TM band 7 is seen in crest dunes parallel with tens of kilometres length. This feature is clear in the northern part of Figure 8 and it is located in high land of DEM of 900 m. This finding confirms the study of Robinson et al. (2007).

Figure 6 shows the lineament distribution with 3-D map reconstruction using SRTM and LANDSAT TM bands 3, 4, 5 and 7. It was clear that the 3-D visualization discriminates between different geological features. The faults, lineament and infrastructures can be noticed clearly

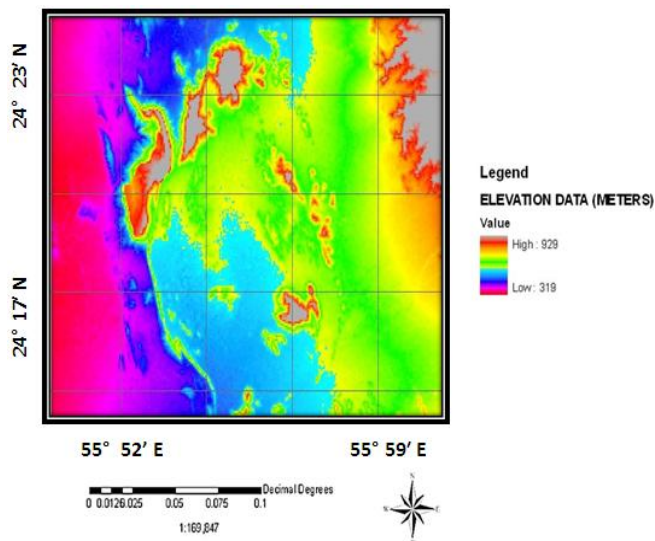


Figure 5. DEM Derived from SRTM data.

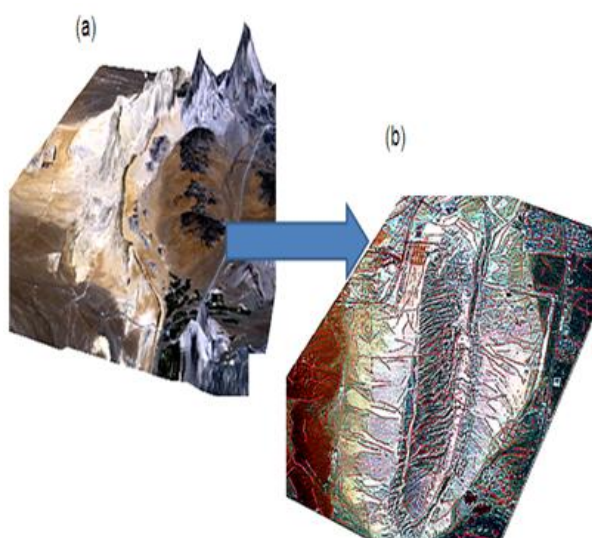


Figure 6. (a) 3D image reconstruction using SRTM data and (b) lineament distribution over 3-D image.

clearly (Figure 6b). This study agrees with that of Marghany et al. (2009). It can be confirmed that the lineaments are associated with faults, and heavy capacity of lineament occurrences is obvious within the Oman mountain. This type of lineament can be named as mountain lineament.

According to Robinson et al. (2007) and Marghany et al. (2009), the mountain is raised higher than 400 m above sea level and exhibit parallel ridges and high-tilted beds. Many valleys cut down the mountains, forming narrow clefts and small caves. The fluvial forms consisted of streams channels which flows from Oman mountains and spread out into several braided channels at the base

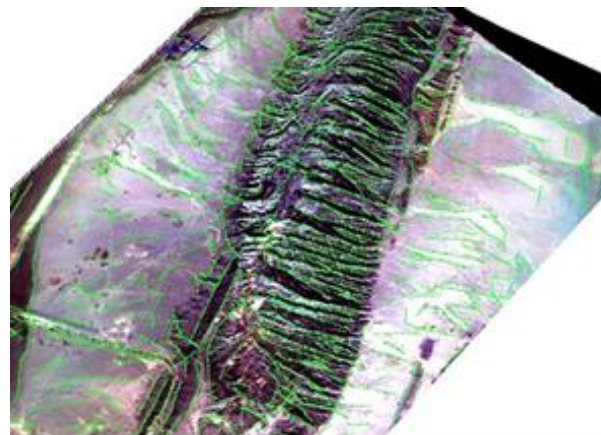
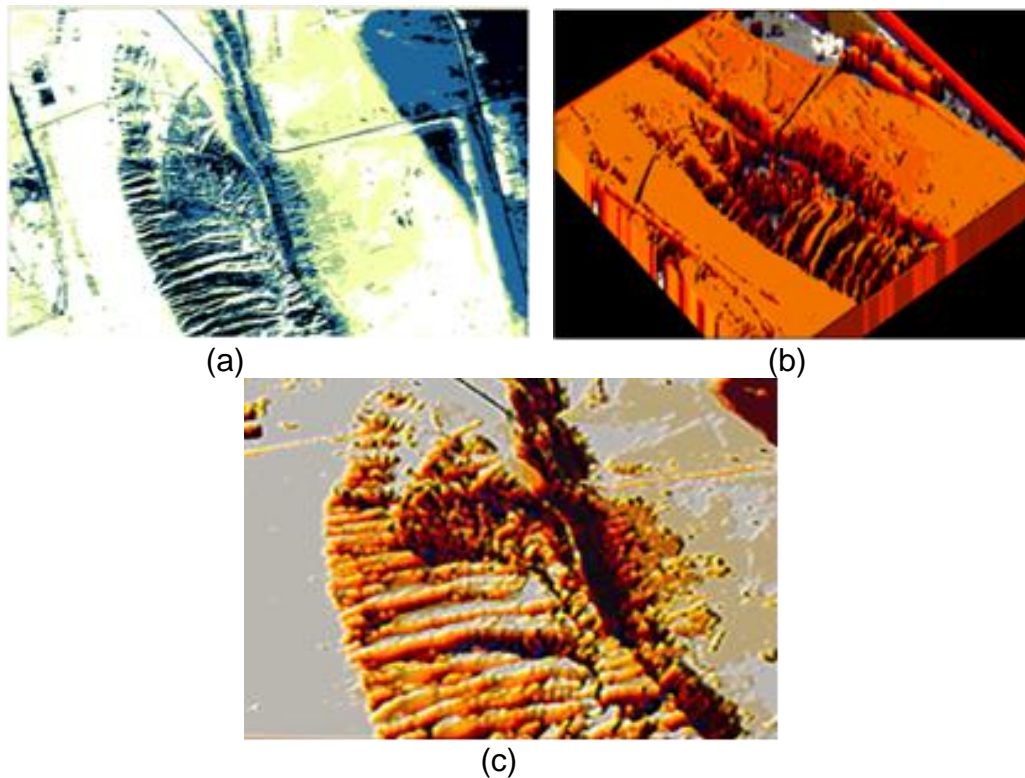


Figure 7. 3-D of lineament distribution derived from Canny algorithm.

of the mountains from the Bahada and Playa plains (Figure 7). Stream channels have been diverted to the southwest and they deposited silt in the tongue-shaped plains which lie between the dunes.

Figure 8 shows the result acquired by using fuzzy B-spline algorithm. It was clear that the 3-D visualization discriminates between different geological features. The faults, lineament and infrastructures can be noticed clearly (Figure 8c). This was due to the fact that the fuzzy B-splines considered as deterministic algorithms which are described here, optimize a triangulation only locally between two different points (Fuchs et al., 1977; Anile et al., 1995; Anile, 1997; Marghany et al., 2010; Marghany and Mazlan, 2011). This corresponds to the feature of deterministic strategies of finding only sub-optimal solutions. The visualization of the geological feature is sharp with the LANDSAT TM satellite image due to the fact that each operation on a fuzzy number becomes a sequence of the corresponding operations on the respective  $\mu$ -levels and the multiple occurrences of the same fuzzy parameters was evaluated as a result of its function on the fuzzy variables (Keppel, 1975; Anile et al., 1995; Marghany and Mazlan, 2011).

It is very easy to distinguish between smooth and jagged features. Typically, in computer graphics, two objective quality definitions for fuzzy B-splines were used: triangle-based criteria and edge-based criteria. Triangle-based criteria of the angles of each triangle follow the rule of maximization or minimization, respectively (Fuchs et al., 1977). The so-called max-min angle criterion prefers short triangles with obtuse angles. This findings confirms those of Keppel (1975) and Anile (1997). Table 1 confirms the accuracy of fuzzy B-spline used to eliminate the uncertainties of 3-D visualization. Consequently, the fuzzy B-spline shows higher performance with standard error of mean of 0.12 and bias of 0.23 than SRTM technique. In fact, fuzzy B-splines provide both a continuous approximating model of the experimental data



**Figure 8.** (a) LANDSAT ETM satellite data and (b) 3D fuzzy B-spline visualization and (c) zoom area of lineaments and fault.

**Table 1.** Statistical comparison of 3-D computer visualization using fuzzy-B-spline and SRTM.

Statistical parameter	3-D visualization	
	Fuzzy B-spline	SRTM
Bias	0.23	0.63
Standard error of the mean	0.12	0.56

and a possibilistic description of the uncertainties in such DEM. Approximation with FBS provides a fast way to obtain qualitatively reliable descriptions whenever the introduction of a precise probabilistic DEM is too costly or impossible. In this study, fuzzy B-spline algorithm produced 3-D lineament visualization without need to ground geological survey. In fact fuzzy B-spline algorithm is able to keep track of uncertainty and provide tool for representing spatially clustered geological features. This advantage of fuzzy B-spline is not provided in Canny algorithm and DEM produced by SRTM data.

## Conclusions

This study has demonstrated new approach to map lineament distributions in UAE using LANDSAT-TM

satellite data. In doing so, 3-D image reconstruction is produced using SRTM data. Then, the Canny algorithm was implemented for lineament automatic detection from LANDSAT TM bands of 3, 4, 5 and 7. The results show that the maximum DEM value of 929 m was found in the northeast direction of UAE. The vegetation covers were dominated by feature in the highest DEM while highlands were located in lowest elevation of 660 m. In addition, Canny algorithm detected automatically lineament and fracture features. Therefore, 3-D visualization discriminated between lineament and fault features. The results show that the highest spatial distribution of lineaments appeared in Oman mountain which was named lineament mountain. In conclusion, the integration between DEM and Canny algorithm can be use as geomatic tool for lineament automatic detection in 3-D visualization. Furthermore, a fuzzy B-spline algorithm

was used to reconstruct 3-D visualization of geologic feature spatial variations with standard error of mean of 0.12 and bias of 0.23. In conclusion, combination between Canny algorithm and DEM generated using fuzzy B-spline could be use as an excellent tool for geologic mapping.

## REFERENCES

- Anile AM (1997). Report on the activity of the fuzzy soft computing group, Technical Report of the Dept. of Mathematics, University of Catania, March 1997, 10 pages.
- Anile AM, Deodato S, Privitera G (1995). Implementing fuzzy arithmetic, Fuzzy Sets and Systems, 72: 123-156.
- Anile AM, Gallo G, Perfilieva I (1997). Determination of Membership Function for Cluster of Geographical data. Genova, Italy: Institute for Applied Mathematics, National Research Council, University of Catania, Italy, October, p. 25. Technical Report No.26/97.
- Canny JA (1986). Computational Approach To Edge Detection. IEEE Transactions on Pattern Analysis and Machine Intelligence. PAMI-8(6): 679-698.
- Deriche R (1987). Using Canny's criteria to derive a recursively implemented optimal edge detector. Int. J. Comp. Vision, 1(2): 167-187.
- Fuchs H, Kedem ZM, Uselton SP (1977). Optimal Surface Reconstruction from Planar Contours. Communications of the ACM, 20: 693-702.
- Islam ABMS, Jameel M, Rahman MA, Jumaat MZ (2011a). Earthquake Time history for Dhaka, Bangladesh as competent seismic record. Int. J. Phys. Sci., 6(16): 3921-3926.
- Islam ABMS, Jameel M, Ahmad SI, Salman FA, and Jumaat MZ (2011b). Engendering earthquake Respons spectra for Dhaka region usable in dynamic analysis of structures. Sci. Res. Ess., 6(16): 3519-3530.
- Islam ABMS, Jameel M, Uddin MA, Ahmad SI (2011c). Simplified design guidelines for seismic base isolation in multi-storey buildings for Bangladesh National Building Code (BNBC). Int. J. Phys. Sci., 6(23): 5467-5486.
- Islam ABMS, Ahmad SI, Jameel M, Jumaat MZ (2012a). Seismic Base Isolation for Buildings in Regions of Low to Moderate Seismicity: A Practical Alternative Design. Pract. Period. Struct. Des. Constr., ASCE, 17(1): 13-20.
- Islam ABMS, Hussain RR, Jameel M, Jumaat MZ (2012b). Non-linear time domain analysis of base isolated multi-storey building under site specific bidirectional seismic loading. Autom. Constr., 22, 554-566.
- Islam ABMS, Jameel M, Jumaat MZ (2012c). Oil and Gas Energy Potential at Malaysian Seabed and Spar Platform for Deepwater Installation. Int. J. Green Energy, 9: 111-120.
- Islam ABMS, Ahmad SI, Jumaat MZ, Hussain RR (2012d). Efficient Design in Building Construction with Rubber Bearing in Medium Risk Seismicity: Case Study & Assessment. J. Civ. Eng. Manag. In Press, Corrected Proof.
- Islam ABMS, Jameel M, Ahmad S, Jumaat MZ, Kurian VJ (2012e). Structural behaviour of fully coupled spar-mooring system under extreme wave loading. J. Civ. Eng. Manag. In Press, Corrected Proof.
- Islam ABMS, Jumaat MZ, Hussain RR, Alam MA (2012f). Incorporation of Rubber-steel Bearing Isolation in Multi-storey Building. J. Civ. Eng. Manag. In Press, Corrected Proof.
- Gonzalez R, Woods R (1992). Digital Image Processing, 3rd edition, Addison-Wesley Publishing Company. pp. 200-229.
- Jameel M, Islam ABMS, Hussain RR, Khaleel M, Zaheer MM (2012a). Optimum structural modelling for tall buildings. Struct Des Tall Spec Build. DOI: 10.1002/tal.1004.
- Jameel M, Ahmad S, Islam ABMS, Jumaat MZ (2012b). Nonlinear dynamic analysis of coupled spar platform. J. Civ. Eng. Manag. In Press, Corrected Proof.
- Jameel M, Islam ABMS, Khaleel M, Amirahmad A (2012c). Efficient three dimensional modeling of high-rise building structures. J. Civ. Eng. Manag. In Press, Corrected Proof.
- Keppel E (1975). Approximation Complex Surfaces by Triangulations of Contour Lines. IBM J. Res. Develop., 19: 2-11.
- Katsuaki K, Shuichi N, Ohmi M (1995). Lineament analysis of satellite images using a segment tracing algorithm (STA). Comp. and Geos., 21(9): 1091-1104.
- Mallast U, Gloaguen R, Geyer S, Rödiger T, Siebert C (2011). Semi-automatic extraction of lineaments from remote sensing data and the derivation of groundwater flow-paths. Hydrol. Earth Syst. Sci. Discuss., 8: 1399-1431.
- Marghany M, Mansor S, Hashim M (2009a). Geologic mapping of United Arab Emirates using multispectral remotely sensed data. Amer. J. Eng. App. Sci., 2: 476-480.
- Marghany M, Hashim M, Crackenal A (2009b). 3D Reconstruction of Coastal Bathymetry from AIRSAR/POLSAR data. Chin. J. Ocean. Lim., 27(1): 117-123.
- Marghany M, Hashim M (2010). Lineament mapping using multispectral remote sensing satellite data. Int. J. Phys. Sci., 5(10): 1501-1507.
- Marghany M, Hashim M, Crackenal A (2010). 3-D visualizations of coastal bathymetry by utilization of airborne TOPSAR polarized data. Int. J. Dig. Eart, 3(2): 187 - 206.
- Mostafa ME, Qari MY (1995). An exact technique of counting lineaments. Eng. Geol., 39: (1-2): 5-15.
- Munir S, Hussain RR, Islam ABMS (2012). Parallel Framework for Earthquake Induced Response Computation of SDOF Structure. J. Civil Eng. Manag. In Press, Corrected Proof.
- Novak ID, Soulakellis N (2000). Identifying geomorphic features using Landsat-5/TM data processing techniques on Ilesvos, Greece. Geom., 34: 101-109.
- Nikolakopoulos KG, Kamaratakis EK, Chrysoulakis N (2006). "SRTM vs ASTER elevation products. Comparison for two regions in Crete, Greece". Int. J. Rem. Sens., 27(21): 4819-4838.
- Russo F (1998). Recent advances in fuzzy techniques for image enhancement. IEEE Trans. on Inst. and meas., 47: 1428-1434.
- Robinson CA, El-Baz F, Kuskyb TM, Mainguet M, Dumayc F, AlSuleimani Z, Al Marjebye A (2007). Role of fluvial and structural processes in the formation of the Wahiba Sands, Oman: A remote Sensing Prospective. J. Arid Env., 69: 676-694.
- Rövid A, Várkonyi AR, Várlaki P (2004). 3D Model estimation from multiple images," IEEE International Conference on Fuzzy Systems, FUZZ-IEEE'2004, July 25-29, 2004, Budapest, Hungary, pp. 1661-1666.
- Semere S, Ghebream W (2006). Lineament characterization and their tectonic significance using Landsat TM data and field studies in the central highlands of Eritrea. J. Afr. Ear. Sci., 46 (4), pp. 371-378.
- Süzen ML, Toprak V (1998). Filtering of satellite images in geological lineament analyses: An application to a fault zone in central Turkey. Int. J. Rem. Sen., 19(6): 1101-1114.
- Walsh GJ, Clark Jr SF (2000). Contrasting methods of fracture trend characterization in crystalline metamorphic and igneous rocks of the Windham quadrangle, New Hampshire. Northeast. Nort. Geol. Env. Sci., 22 (2): 109-120.
- Zaineldeen U (2011). Paleostress reconstructions of Jabal Hafit structures, Southeast of AlAin City, United Arab Emirates (UAE). J. Afr. Ear. Sci., 59:323-335.